Magnetic ordering and superconductivity in the $R_2Ir_3Ge_5$ (R=Y, La, Ce–Nd, Gd–Tm, Lu) system

Yogesh Singh and S. Ramakrishnan
Tata Institute of Fundamental Research, Bombay-400005, India
(Received 13 October 2003; revised manuscript received 1 March 2004; published 25 May 2004)

We report crystal structure, electrical resistivity, magnetic susceptibility, isothermal magnetization, and heat-capacity studies on polycrystalline samples of the intermetallic series $R_2Ir_3Ge_5$ (R=Y, La, Ce–Nd, Gd–Tm, Lu) from 1.5 to 300 K. We find that the compounds for R=Y, La-Dy, crystallize in the tetragonal *Ibam* ($U_2Co_3Si_5$ type) structure whereas the compounds for R=Er–Lu, crystallize in a different orthorhombic structure with a space group *Pmmn*. Samples of $Ho_2Ir_3Ge_5$ were always found to be multiphase. The compounds for R=Y–Dy which adopt the *Ibam* type structure show a metallic resistivity with a tendency of saturation at high temperatures whereas the compounds with R=Er, Tm, and Lu show an anomalous behavior in the resistivity with a semiconducting increase in ρ as we go down in temperature from 300 K. Interestingly we had earlier found a positive temperature coefficient of resistivity for the Yb sample in the same temperature range. We will compare this behavior with similar observations in the compounds $R_3Ru_4Ge_{13}$ and RBiPt. $La_2Ir_3Ge_5$ and $Y_2Ir_3Ge_5$ show bulk superconductivity below 1.8 K and 2.5 K, respectively. Our results confirm that $Ce_2Ir_3Ge_5$ shows a Kondo-lattice behavior and undergoes antiferromagnetic ordering below 8.5 K. Most of the other compounds containing magnetic rare-earth elements undergo a single antiferromagnetic transition at low temperatures ($T \leqslant 12$ K) while $Gd_2Ir_3Ge_5$, $Dy_2Ir_3Ge_5$, and $Nd_2Ir_3Ge_5$ show multiple transitions. The T_N's for most of the compounds roughly scale with the de Gennes factor, which suggests that the primary mechanism of interaction leading to the magnetic ordering of the magnetic moments may be the Ruderman-Kittel-Kasuya-Yosida interaction. The ordering temperature of 8.5 K for $Ce_2Ir_3Ge_5$ is anomalously large compared to the T_N for $Gd_2Ir_3Ge_5$ which is about 12 K. There are signs of strong CEF influence on the measured properties for the series.

DOI: 10.1103/PhysRevB.69.174423 PACS number(s): 74.70.Ad, 74.25.Bt, 74.25.Ha

I. INTRODUCTION

Rare-earth ternary silicides and germanides of the type $R_2T_3X_5$, where T is a transition metal and X is either Si or Ge have been extensively investigated for their unusual magnetic and superconducting properties and the rich variety of crystal structures they form in Refs. 1–5. In particular, compounds belonging to the $R_2Fe_3Si_5$ series have prompted considerable efforts to understand their superconductivity and magnetism.[5–8] Both $Tm_2Fe_3Si_5$ and $Lu_2Fe_3Si_5$ compounds show superconductivity at low temperatures. In the Tm sample, superconductivity at about 1.5 K is destroyed by the onset of antiferromagnetic order at 1 K and it reenters the normal state[9] whereas $Lu_2Fe_3Si_5$ has the highest T_C=6 K for an iron containing compound.[10] Recently it was reported that $Er_2Fe_3Si_5$ was also found to be superconducting below 1 K.[11] In this crystal structure, Fe does not have any moment and it only helps in building up the large density of states at the Fermi level. Recently we have established $Yb_2Fe_3Si_5$ to be a heavy fermion compound with Kondo-Lattice behavior and antiferromagnetic ordering below 1.7 K.[12] Thus it is clear that compounds of the series $R_2Fe_3Si_5$ exhibit unusual superconducting and magnetic properties. The $R_2Ir_3Ge_5$ series of compounds formed in a crystal structure which is closely related to the $R_2Fe_3Si_5$ structure. The compound $Ce_2Ir_3Ge_5$ of this series has been studied in some detail by various groups[13–15] but there have been little efforts to make a detailed study of the other compounds of the series $R_2Ir_3Ge_5$. Recently we had succeeded in preparing and studying the compound $Yb_2Ir_3Ge_5$. We found that apart from showing interesting low-temperature properties[16] it also formed in a crystal structure different from its Ce analog. This prompted us to make a comprehensive study of the structural and magnetic properties of the complete $R_2Ir_3Ge_5$ series to look for systematic trends and variations in the physical properties across the series. Here we report our detailed resistivity, magnetic susceptibility, isothermal magnetization, and heat-capacity results for the series $R_2Ir_3Ge_5$ (R=Y, La, Ce–Nd, Gd–Tm, Lu) from 1.5 to 300 K.

II. EXPERIMENTAL DETAILS

Samples of $R_2Ir_3Ge_5$ (R=Y, La–Nd, Gd–Tm, Lu) were made by melting the individual constituents (taken in stoichiometric proportions) in an arc furnace under Ti gettered high-purity argon atmosphere on a water cooled copper hearth. The purity of the rare-earth metals and Ir was 99.9% whereas the purity of Ge was 99.999%. The alloy buttons were flipped over and remelted five to six times to ensure homogeneous mixing. The samples were annealed at 950 °C for a period of 10 days before slowly cooling down to room temperature. The x-ray powder diffraction pattern of the samples did not show the presence of any parasitic impurity phases. The samples with R=Y, La, Ce–Dy, were found to adopt the tetragonal *Ibam* ($U_2Co_3Si_5$ type) crystal structure as reported earlier for the compound $Ce_2Ir_3Ge_5$ (Ref. 15) whereas the compounds for R=Er–Lu, crystallize in an orthorhombic crystal structure with a space group *Pmmn*

TABLE I. Lattice parameters of $R_2Ir_3Ge_5$.

Sample	a (Å)	b (Å)	c (Å)
$Y_2Ir_3Ge_5$	10.121±0.005	11.802±0.005	5.950±0.005
$La_2Ir_3Ge_5$	10.246±0.005	12.851±0.005	6.104±0.005
$Ce_2Ir_3Ge_5$	10.241±0.005	12.019±0.005	6.094±0.005
$Pr_2Ir_3Ge_5$	10.236±0.005	11.986±0.005	6.074±0.005
$Nd_2Ir_3Ge_5$	10.229±0.005	11.968±0.005	6.064±0.005
$Gd_2Ir_3Ge_5$	10.224±0.005	11.843±0.005	6.032±0.005
$Tb_2Ir_3Ge_5$	10.219±0.005	11.802±0.005	5.997±0.005
$Dy_2Ir_3Ge_5$	10.214±0.005	11.783±0.005	5.984±0.005
$Er_2Ir_3Ge_5$ [a]	19.062±0.005	15.679±0.005	4.633±0.005
$Tm_2Ir_3Ge_5$ [a]	18.998±0.005	15.580±0.005	4.612±0.005
$Lu_2Ir_3Ge_5$ [a]	18.901±0.005	15.382±0.005	4.567±0.005

[a]Different structure (see text).

which we had recently reported[16] for the sample $Yb_2Ir_3Ge_5$. The x-ray pattern for the sample $Ho_2Ir_3Ge_5$ always showed many extra reflections which shows that Ho was the transition point for the structural change. We also found that the Ho x-ray pattern was not just a simple mixture of *Ibam* and *Pmmn* although many lines could be indexed to one or the other of these two structures. The third (or possibly more) phase could not be identified at present. Although the x ray for the sample $Er_2Ir_3Ge_5$ did not show any extra peaks, preliminary EPMA study showed the presence of a small amount of second phase. The lattice constants a, b, and c obtained from least-square fits of the x-ray patterns are listed in Table I where the $Y_2Ir_3Ge_5$ sample is seen to have smaller lattice parameters than the La sample as expected and then they (a, b, and c) are seen to decrease linearly across the series from $La_2Ir_3Ge_5$ to $Dy_2Ir_3Ge_5$ (*Ibam* structure) and from $Er_2Ir_3Ge_5$ to $Lu_2Ir_3Ge_5$ (*Pmmn* structure). The $U_2Co_3Si_5$ structure has only a single site for U whereas the *Pmmn* crystal structure allows two sites for the rare-earth element. Hence, the net hybridization between *d*- and *f*- orbitals can be very different for these two crystal structures which has to be taken into account in the analysis of magnetic ordering temperatures.

The temperature dependence of dc susceptibility (χ) was measured using a commercial superconducting quantum interference device magnetometer in the temperature range from 1.8 to 300 K. The ac susceptibility was measured using a home-built susceptometer[17] from 1.5 to 20 K. The absolute accuracy with which magnetization measurements were performed is within 1%. The resistivity was measured using an ac resistance bridge (Linear Research Inc., USA) from 1.5 to 300 K. We used a four-probe dc technique with contacts made using silver paint on thin slides cut from the annealed samples. The temperature was measured using a calibrated Si diode (Lake Shore Inc., USA) sensor. All the data were collected using an IBM compatible PC/AT via IEEE-488 interface. The relative accuracy of the resistance measurements is 50 ppm while the accuracy of the absolute resistivity is only 5% due to errors in estimating the geometrical factors. The heat capacity in zero field between 1.7 and 30 K was measured with an accuracy of 1% using an automated adiabatic heat pulse calorimeter. A calibrated germanium resistance thermometer (Lake Shore Inc., USA) was used as the temperature sensor in this range.

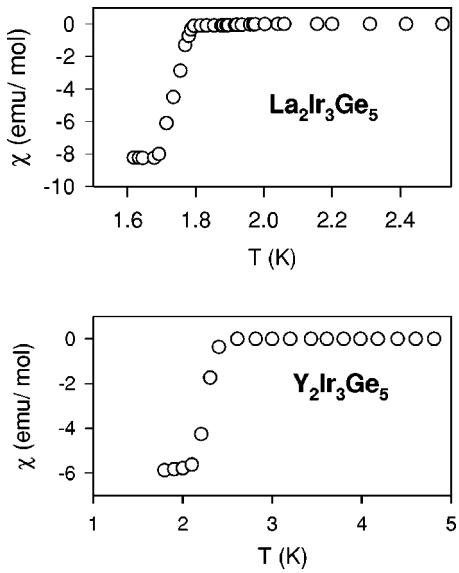

FIG. 1. Variation of susceptibility (χ) of $La_2Ir_3Ge_5$ and $Y_2Ir_3Ge_5$ down to 1.5 K in a field of 1 mT showing the diamagnetic drop at the respective superconducting transition temperatures. No diamagnetism was seen for $Lu_2Ir_3Ge_5$ (see text for details of the high-temperature behavior).

III. RESULTS

A. Magnetic susceptibility and magnetization studies

1. Properties of $Y_2Ir_3Ge_5$, $La_2Ir_3Ge_5$, and $Lu_2Ir_3Ge_5$

The low-temperature dependence of the dc magnetic susceptibility (χ) of $La_2Ir_3Ge_5$ and $Y_2Ir_3Ge_5$ are shown in Fig. 1. The panel for $La_2Ir_3Ge_5$ clearly shows an abrupt diamagnetic drop just below 1.75 K which marks the onset of the sample into the superconducting state. In the normal state (not shown here) the χ of $La_2Ir_3Ge_5$ is diamagnetic between 75 and 300 K but shows a Curie-Weiss like tail as we go down in temperature. It is possible that there is a small amount of magnetic impurity in La or Ir metals. However, the susceptibility χ for both the Y and Lu samples (not shown here) are practically temperature independent down to low temperatures with only small upturns at the lowest temperatures (probably due to paramagnetic impurities) hence the possibility of Ir having a significant amount of impurity is remote. For $Y_2Ir_3Ge_5$, a somewhat sharper diamagnetic transition below 2.5 K as seen in the lower panel of the figure signals the transition into the superconducting state for this compound. We did not observe any diamagnetic signal down to 1.8 K for $Lu_2Ir_3Ge_5$.

2. Properties of $R_2Ir_3Ge_5$ (R=Ce–Dy)

The temperature dependence of the inverse dc magnetic susceptibility (χ^{-1}) of the magnetic $R_2Ir_3Ge_5$ (R =Ce–Nd, Gd–Dy, Er, and Tm) is shown in Fig. 2. The high-temperature susceptibility (100 K$<T<$300 K) for all

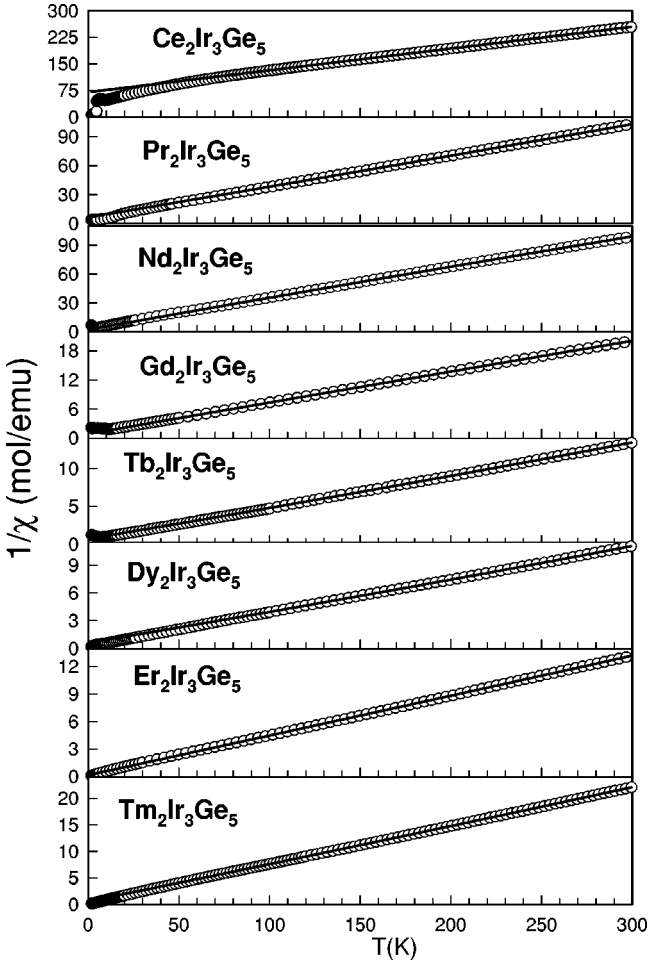

FIG. 2. Variation of inverse dc susceptibility ($1/\chi$) of the magnetic samples $R_2Ir_3Ge_5$ (R=Ce–Nd, Gd–Tm) from 1.8 to 300 K in a field of 0.1 T. The solid line is a fit to the Curie-Weiss relation (see text for details).

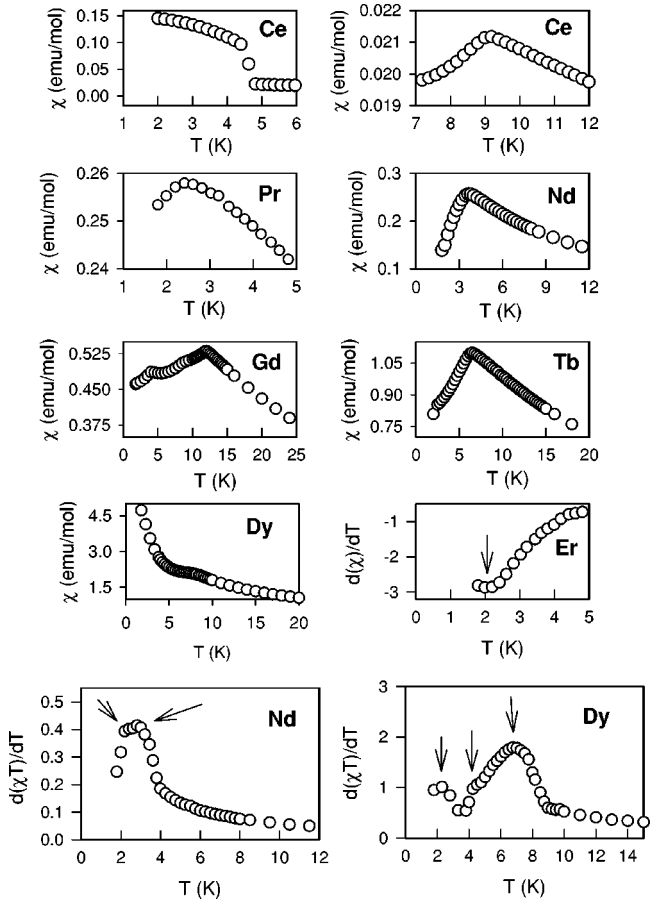

FIG. 3. The low temperature χ or $d\chi T/dT$ vs T behavior for all the magnetic samples (except Tm which does not order down to 1.7 K) on an expanded scale to highlight the respective magnetic transitions. The multiple anomalies marked by arrows for some samples are best brought out by plotting the derivative of the susceptibility vs T (see text for details).

the magnetic members of the series could be fitted to a modified Curie-Weiss expression which is given by

$$\chi = \chi_0 + \frac{C}{(T-\theta_p)}, \tag{1}$$

where C is the Curie constant which can be written in terms of the effective moment as

$$C(\text{emu K/mol}) = \frac{N_a(\mu_{eff})^2(\mu_B)^2}{3\ K_B} \approx \frac{(\mu_{eff})^2(\mu_B)^2\ x}{8}, \tag{2}$$

where x is the number of magnetic R ions per formula unit. The resulting fit is also shown in the Fig. 2. The values of χ_0, μ_{eff}, and θ_p are given in Table I. The main contributions to the temperature independent χ_0 are, namely, the diamagnetic susceptibility which arises due to the presence of ion cores, the Pauli spin susceptibility of the conduction electrons, and the Landau diamagnetism. The estimated effective moment in all the cases is found to be quite close to the free ion moment of R^{3+} ion telling us that we are dealing with trivalent rare-earth ions here. For most of the compounds (except $Ce_2Ir_3Ge_5$), we get a relatively small and negative value of the Curie-Weiss temperature (θ_p). A negative θ_p implies the presence of antiferromagnetic correlations. For $Ce_2Ir_3Ge_5$, we obtain a negative and large value of $\theta_p = -137$ K indicating a strong hybridization of $4f$ orbitals of Ce which leads to a high Kondo temperature as we will see when we discuss the resistivity results. This is in agreement with an earlier report[15] which also estimated a large value of -160 K for θ_p. The value of θ_p for most of the other samples is between -10 K and -20 K which although smaller than the value for $Ce_2Ir_3Ge_5$, is still somewhat larger than, e.g., the values obtained for the compounds of the series $R_2Rh_3Sn_5$.[18]

The low temperature $\chi(T)$ and/or $d\chi(T)/dT$ data for all the magnetic samples (except Tm which does not order down to 1.8 K) is shown in Fig. 3. The anomalies in the low-temperature susceptibility clearly show the antiferromagnetic ordering for all the compounds. For $Ce_2Ir_3Ge_5$, we also observe an abrupt upturn in the susceptibility below 4.5 K after the sample has undergone an antiferromagnetic transition at 8.5 K. This upturn in χ below T_N was also observed in an earlier work.[19] There are no signatures of this transition in

TABLE II. Parameters obtained from the high-temperature susceptibility fit to the Curie-Weiss expression given by the Eq. (1). μ_{th} is theoretical free ion value.

Sample	χ_0 emu/mol K	μ_{eff} μ_B	μ_{th} μ_B	θ_p (K)
$La_2Ir_3Ge_5$	-1.76×10^{-3}			
$Ce_2Ir_3Ge_5$	3.579×10^{-4}	2.535	2.54	-113.2
$Pr_2Ir_3Ge_5$	-2.119×10^{-4}	3.567	3.58	-20.69
$Nd_2Ir_3Ge_5$	3.842×10^{-4}	3.46	3.62	-7.57
$Gd_2Ir_3Ge_5$	6.498×10^{-4}	7.856	7.94	-13.91
$Tb_2Ir_3Ge_5$	-1.375×10^{-3}	9.79	9.7	-14.02
$Dy_2Ir_3Ge_5$	-2.332×10^{-3}	11.09	10.65	-18.85
$Er_2Ir_3Ge_5$	-6.964×10^{-4}	9.64	9.59	-3.813
$Tm_2Ir_3Ge_5$	-1.532×10^{-3}	7.6	7.56	-8.99
$Lu_2Ir_3Ge_5$	$-2.\times10^{-4}$			
$Y_2Ir_3Ge_5$	2.9×10^{-4}			

the resistivity but there is a weak kink in the heat-capacity data. This feature seen in both the magnetic susceptibility and heat-capacity measurements could be intrinsic to the sample or may be due to a small ferromagnetic impurity phase. Microanalysis studies are needed to verify whether this behavior is intrinsic to the sample. The low-temperature χ data for $Gd_2Ir_3Ge_5$ also shows a second shoulder like feature around 4.5 K apart from the antiferromagnetic transition at about 12 K. We will later see that two anomalies are also observed in the resistivity and heat-capacity data for this sample. The transition temperatures of various compounds obtained from magnetic susceptibility measurements are listed in Table II. The ordering temperatures have been determined from peaks/inflection points in the $d(\chi T)/dT$ vs T plots. The $d(\chi T)/dT$ vs T plots for $Nd_2Ir_3Ge_5$ and $Dy_2Ir_3Ge_5$ showed additional anomalies apart from the single transition visible in the $\chi(T)$ data. This can be seen (marked by arrows) in the bottom most panels of Fig. 3 where we show the $d(\chi T)/dT$ vs T plots for $Nd_2Ir_3Ge_5$ and $Dy_2Ir_3Ge_5$. Thus it can be seen that $Nd_2Ir_3Ge_5$ shows two anomalies at 2.1 K and 2.82 K while $Dy_2Ir_3Ge_5$ shows three anomalies at 2, 4.3, and 7.2 K. We will later show that these multiple anomalies are also observed in the resistivity and heat-capacity measurements for these samples. The $d(\chi)/dT$ plot for $Er_2Ir_3Ge_5$, shown in the same Fig. 3, also shows a minima just around 2 K which could be a possible signature of magnetic order. This is corroborated by anomalies at the same temperature in the resistivity and heat-capacity data which we will discuss below.

3. Magnetization studies of $R_2Ir_3Ge_5$ ($R=Ce-Nd$, $Gd-Dy$)

Isothermal magnetization measurements at temperatures both above and below the Neel temperature T_N have been performed on the samples undergoing magnetic order. Figure 4 shows the magnetization curves for the samples $Ce_2Ir_3Ge_5$, $Pr_2Ir_3Ge_5$, $Nd_2Ir_3Ge_5$, $Gd_2Ir_3Ge_5$, $Tb_2Ir_3Ge_5$, and $Dy_2Ir_3Ge_5$. We observe a nonlinear behavior in M vs H at 2 K ($<T_N$) for all the samples. This nonlinear behavior agrees with the notion of antiferromagnetic ordering of R^{3+}

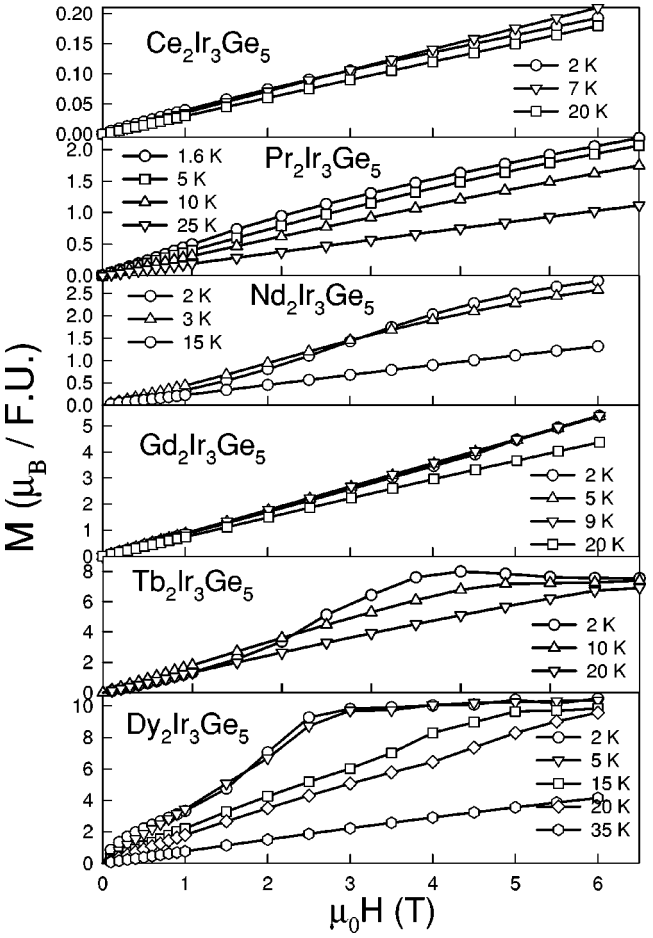

FIG. 4. Isothermal magnetization (M) of $R_2Ir_3Ge_5$ (R = Ce, Pr, Nd, Gd, Tb, and Dy) vs magnetic field (H) at various temperatures. The nonlinearity in M vs H at temperatures below T_N agrees with the notion of antiferromagnetic ordering of R^{3+} spins whereas the linear dependence of M on H above T_N (except for $Tb_2Ir_3Ge_5$ and $Dy_2Ir_3Ge_5$) signifies that the sample is in the paramagnetic state at this temperature.

spins. This nonlinear behavior persists up to 7 K in the case of Ce compound. At higher temperatures ($T>T_N$), one observes the usual linear behavior (except for the Tb and Dy samples which show a curvature even for temperatures above T_N) in magnetization which characterizes the paramagnetic state. The magnetization values of Ce are very small presumably due to the presence of Kondo effect. The magnetization for $Pr_2Ir_3Ge_5$ at 1.8 K and 5 K starts out linearly but shows a curvature for higher fields. Above 10 K the linear behavior is observed. The magnetization data for $Gd_2Ir_3Ge_5$ at 2 K starts out linearly up to 1 T but shows a slight upturn at higher fields which continues up to 6 T with no sign of saturation. A similar behavior is observed for other temperatures below $T_N(=12$ K). At 20 K the magnetization is linear upto the highest fields with a slightly smaller slope than the curve at 2 K. The magnetization data of Nd, Tb, and Dy at 2 K show an S type of shape with increasing field. The magnetization for $Nd_2Ir_3Ge_5$ at 2 K starts out linearly but begins to show an upturn starting at 1.5 T which continues up to a field of 4 T after which it shows signs of saturating at higher

fields reaching a value of $2.77\mu_B$/f.u. which is slightly lower than the value of $3.27\mu_B$/f.u. for Nd^{3+} saturated moments. Higher fields may be required to reach the full moment value since the magnetization has not completely saturated even for the highest field (=6 T) used in our measurements. A similar behavior is also seen in the magnetization curve at 3 K. At 15 K, we get the linear behavior expected in the paramagnetic state. The magnetization for $Tb_2Ir_3Ge_5$ at 2 K starts out linear but shows an upward curvature for fields higher than 1 T. At higher fields it saturates reaching a value of $7.6\mu_B$/f.u. which is lower than $9\mu_B$/f.u. expected for Tb^{3+} saturated moments. This behavior is also seen at 10 K which is higher than T_N for this compound. This indicates possible short-range magnetic correlations even above T_N. A linear behavior is again obtained at 20 K. The magnetization for $Dy_2Ir_3Ge_5$ at 2 K and 5 K starts out with a slightly sublinear behavior at low fields up to about 1 T after which it begins to curve upwards up to a field of 2.5 T. For higher fields it sort of saturates, reaching a value of about $10.4\mu_B$/f.u. at 6 T which is close to the free moment value of $10\mu_B$/f.u. for Dy^{3+} moments. A similar behavior for the magnetization with saturation at 5 T is seen at a temperature of 15 K which is much above the Neel temperature of 7 K for $Dy_2Ir_3Ge_5$. A linear behavior for the magnetization is seen only at 35 K. Clearly there are short-range magnetic correlations even above T_N in this compound and this aspect would be worth further investigation prefrably by neutron scattering experiments.

B. Resistivity studies on $R_2Ir_3Ge_5$ (R=Y, La–Tm)

The resistivity data (ρ) for $La_2Ir_3Ge_5$ and $Y_2Ir_3Ge_5$ is shown in Fig. 5. The insets show the low-temperature data which clearly show a sharp drop in the resistivity marking the onset of the superconducting transitions for both the samples below 1.7 K and 2.4 K, respectively. This drop corresponds with the diamagnetic signal observed in the susceptibility measurement for both the samples. An earlier report[15] did not find any superconductivity for $La_2Ir_3Ge_5$. However, their investigations had been carried out only down to 1.8 K below which we observe the resistive drop and diamagnetic signal in the susceptibility. We will later see that we also observe an incomplete peak at roughly the same temperature in the heat-capacity measurements. The resistivity $[\rho(T)]$ for the samples with R=Ce–Dy is shown in Fig. 6. The top panel shows the resistivity data for the Ce, Pr, Gd, Tb, and Dy samples between 1.5 K and 300 K. The resistivity of the Nd sample lies very close to the Pr sample data and hence is not shown for clarity. The small panels in the same figure show the low temperature ρ or $d\rho T/dT$ data for the Ce–Dy samples. One can see that the resistivity data of all the magnetic rare-earth samples except that of $Pr_2Ir_3Ge_5$ show a change of slope at their respective magnetic transitions at roughly the same temperatures where anomalies are seen in the susceptibility measurements. It can be seen that for the $Gd_2Ir_3Ge_5$ and $Dy_2Ir_3Ge_5$ samples, plotting $d(\rho)T/dT$ vs T brings out the third anomaly in $Dy_2Ir_3Ge_5$ and the second anomaly in $Gd_2Ir_3Ge_5$ which were not present in the $\rho(T)$ data. However, taking $d(\rho)/dT$ for $Nd_2Ir_3Ge_5$ did not help

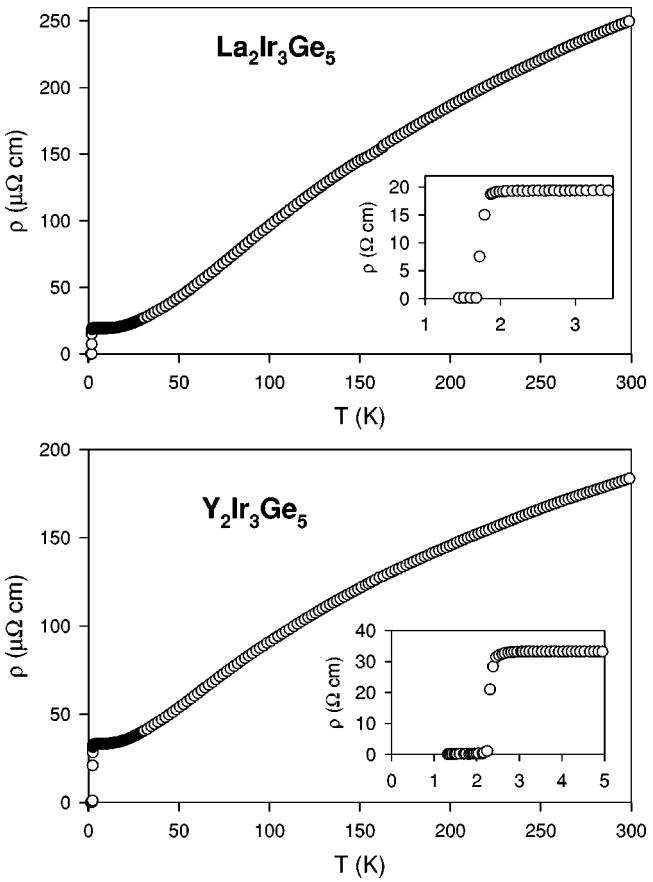

FIG. 5. Temperature dependence of resistivity (ρ) of $R_2Ir_3Ge_5$ (R=Y and La) from 1.5 to 300 K. The insets show the low temperature ρ data. The superconducting transitions can be clearly seen for both $La_2Ir_3Ge_5$ and $Y_2Ir_3Ge_5$.

because it was very noisy and possibly the two transitions are very close together in temperature (as will be seen in the discussion of the heat capacity for this sample) and may not be individually distinguishable in the resistivity data. Figure 7 shows the temperature dependence of resistivity data for $Er_2Ir_3Ge_5$, $Tm_2Ir_3Ge_5$, and $Lu_2Ir_3Ge_5$ which crystallize in the orthorhombic *Pmmn* structure. It is evident from the top panel in this figure that the ρ behavior for these compounds is anomalous showing a semiconducting rise of ρ for all three compounds as we cool down from 300 K. It is interesting to note that we had found a positive temperature coeffecient of the resistivity for the sample $Yb_2Ir_3Ge_5$ (Ref. 16) in the same temperature range. Similar behavior for the resistivity has been observed earlier for the series of compounds $R_3Ru_4Ge_{13}$ (Ref. 20) and RBiPt (Ref. 21) where the resistivity for all samples except Yb showed a semiconducting response. The lower left side panels in Fig. 7 show the low-temperature data for the Er, Tm, and Ku samples individually. The $Er_2Ir_3Ge_5$ data is highly anomalous in the sense that it initially increases with decreasing temperature like its isostructural neighbors Tm and Lu but then it reaches a broad maximum at nearly 100 K before starting to decrease more or less linearly with temperature. The resistivity then shows an upturn at about 5 K (see the smaller panel for the Er sample) before decreasing abruptly below 2 K indicating

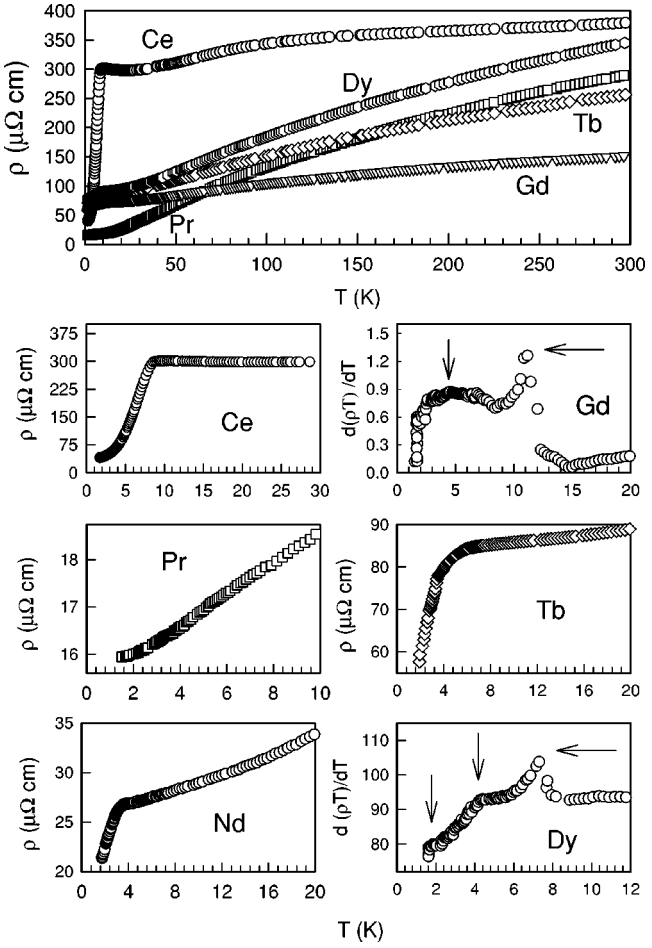

FIG. 6. Temperature dependence of resistivity (ρ) of $R_2Ir_3Ge_5$ (R=Ce–Nd, Gd–Dy). The large panel at the top shows the data from 1.5 K to 300 K. The small panels below show the low temperature ρ or $d\rho T/dT$ data to highlight the anomalies at the magnetic transitions for the individual samples.

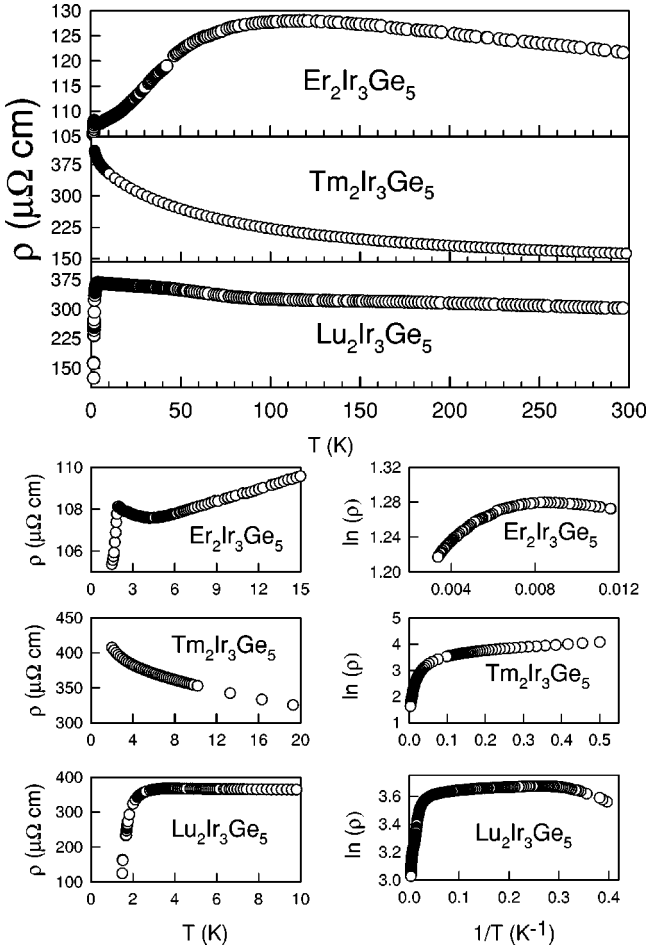

FIG. 7. Temperature dependence of resistivity (ρ) of $R_2Ir_3Ge_5$ (R=Er, Tm, and Lu) from 1.5 to 300 K is shown in the top multipanel figure. The ρ vs T behavior at low temperatures is shown in the small panels in the bottom left side of the figure. The ln(ρ) vs T data is shown in the three small panels on the bottom right side of the figure. The ln(ρ) vs T plots show the absence of an activated behavior for the resistivity of these samples (see discussion for details).

a possible magnetic ordering. Evidence of magnetic order has earlier been seen in the $d\chi/dT$ vs T plot which showed an anomaly at 2 K and we will later see that the heat capacity for this sample also shows a peak around 2 K. There is no evidence of any ordering in the resistivity data for $Tm_2Ir_3Ge_5$ down to 1.8 K. There is an abrupt drop of almost 70% in the ρ for $Lu_2Ir_3Ge_5$ below 2 K which may possibly be the onset of superconductivity although the resistivity does not fall completely to zero. Our heat-capacity data also shows an incomplete anomaly just below 2 K as will be discussed later. The $\ln\rho$ vs $1/T$ plots shown in the smaller panels on the lower right-hand side of the same figure will be explained in the section where we discuss our results. The transition temperatures observed from resistivity data are compared with those obtained from susceptibility and heat-capacity studies (described later) in Table II.

In the normal state, i.e., above the superconducting/magnetic transition temperatures, we have been able to fit the low-temperature (T_C or T_N to 25 K) dependence of ρ to a power law which can be written as

$$\rho = \rho_0 + aT^n. \quad (3)$$

The values of ρ_0, a, and n are given in Table III. For $La_2Ir_3Ge_5$ and $Y_2Ir_3Ge_5$, the optimum value of n was found to be 3.6 and 3.3, respectively. These values do not agree with Wilson's s-d scattering model which predicts a T^3 dependence of $\rho(T)$ for $T<\theta_D/10$.[22] The discrepancy could arise due to a variety of reasons such as, complex structure of the Fermi surface, phonon-drag effects, and lattice anharmonicity.

The ρ of most of the magnetic rare-earth samples (except $Ce_2Ir_3Ge_5$) shows a power-law dependence in the low-temperature paramagnetic region ($T_N<T<25$ K) with n different from Eq. (2) in all cases except for $Gd_2Ir_3Ge_5$. The value of n for both $Tb_2Ir_3Ge_5$ and $Dy_2Ir_3Ge_5$ is nearly equal to 2.1, however, the values for $Pr_2Ir_3Ge_5$ ($n=2.4$) and $Nd_2Ir_3Ge_5$ ($n=1.7$) deviate markedly from the T^2 dependence and are not understood at present.

At high temperatures (75 K$<T<$300 K), the resistivity data (for R =Y, La, Ce–Dy) deviate significantly from the expected linear temperature dependence and show a ten-

TABLE III. Transition temperatures T_p (T_N or/and T_{sc}) obtained from different measurement techniques. Most of them are T_N values except for Y, La, and Lu compounds.

Sample	From χ	From ρ	From C_p
	T_p (K)	T_p (K)	T_p (K)
$Y_2Ir_3Ge_5$	2.6 [a]	2.65 [a]	2.48 [a]
$La_2Ir_3Ge_5$	1.74 [a]	1.7 [a]	1.75 [a]
$Ce_2Ir_3Ge_5$	8.9	8.5	8.7
$Pr_2Ir_3Ge_5$	2.1		2.04
$Nd_2Ir_3Ge_5$	2.1,2.82	3	2.08,2.75
$Gd_2Ir_3Ge_5$	4.4,11.9	4.2,11.5	4.5,11.21
$Tb_2Ir_3Ge_5$	6.4	5.9	6.0
$Dy_2Ir_3Ge_5$	2.0,4.3,7.2	1.98,4.7,7.8	2.07,4.79,7.3
$Er_2Ir_3Ge_5$		1.97	1.91
$Tm_2Ir_3Ge_5$			
$Lu_2Ir_3Ge_5$		1.94 [b]	1.85 [b]

[a]Superconducting transition (T_c).

[b]Onset of superconductivity. The transition is not complete.

dency to saturate. This has been seen in many compounds where the value of ρ becomes sufficiently large for the mean-free path to shorten to the order of a few atomic spacings. When that happens, the scattering cross section will no longer be linear in the scattering perturbation. Since the dominant temperature-dependent scattering mechanism is electron-phonon interaction here, the ρ will no longer be proportional to the mean-square atomic displacement, which is proportional to T for a harmonic potential. Instead, the resistance will rise less rapidly than linearly in T and will show negative curvature ($d^2\rho/dT^2 < 0$). This behavior was also seen in our previous studies on silicides and germanides.[4,18]

One of the models which describe the high temperature $\rho(T)$ of these compounds is known as the parallel resistor model.[23] In this model the expression of $\rho(T)$ is given by,

$$\frac{1}{\rho(T)} = \frac{1}{\rho_1(T)} + \frac{1}{\rho_{max}}, \tag{4}$$

where ρ_{max} is the temperature independent saturation resistivity and $\rho_1(T)$ is the ideal temperature-dependent resistivity. Further, the ideal resistivity is given by the following expression:

$$\rho_1(T) = \rho_0 + C_1\left(\frac{T}{\theta_D}\right)^3 \int_0^{\theta_D/T} \frac{x^3 dx}{[1-\exp(-x)][\exp(x)-1]}, \tag{5}$$

where ρ_0 is the residual resistivity and the second term is due to phonon-assisted electron scattering similar to the s-d scattering in transition metal compounds. θ_D is the Debye temperature and C_1 is a numerical constant. The origin of ρ_{max} in this model can be qualitatively explained by noting that infinite scattering can only bring the mean-free path down to an average interatomic spacing and not lower than that because one may be reasonable in saying that the electrons are scattered at most at every atom. Thus the resistance will tend to attain a saturation value ρ_{max}.

TABLE IV. Parameters obtained from the low-temperature resistivity fit of $R_2Ir_3Ge_5$.

Sample	ρ_0 $\mu\Omega$ cm	a $n\Omega$ cm/K^n	n n
$La_2Ir_3Ge_5$	19.35	0.037	3.6
$Y_2Ir_3Ge_5$	33.17	0.12	3.28
$Pr_2Ir_3Ge_5$	16.71	6.71	2.42
$Nd_2Ir_3Ge_5$	27.5	45	1.71
$Gd_2Ir_3Ge_5$	73.35	4	2
$Tb_2Ir_3Ge_5$	84.85	7.30	2.12
$Dy_2Ir_3Ge_5$	88.47	9.59	2.12

The high temperature (75 K$<T<$300 K) ρ data of the samples with R=Y, La–Dy (which show metallic behavior) could be fitted nicely to the parallel resistor model. The values of the various parameters obtained from the fit to this model are listed in Table IV. The θ_D values estimated from fitting the heat-capacity data (discussed below) are also given in Table IV. No attempt was made to fit the parallel resistor model to the ρ data of $Ce_2Ir_3Ge_5$ since this compound exhibits Kondo behavior.

C. Heat-capacity studies on $R_2Ir_3Ge_5$ (R=La–Tm, Lu, Y)

The temperature dependence of the heat capacity from 1.8 to 30 K of various compounds of the series $R_2Ir_3Ge_5$ are shown in Figs. 8, 9, and 10. The main figure shows the magnetic contribution (C_{mag}) to the heat capacity and the estimated entropy (S_{mag}). The C_P data has been omitted for clarity. The insets show the C_{mag}/T (C_P/T for nonmagnetic samples) vs T^2 data at low temperatures to highlight the anomalies at the various transitions for the respective samples. For the magnetic samples $R_2Ir_3Ge_5$ (R=Ce–Dy), we had a choice to use either $La_2Ir_3Ge_5$ or $Y_2Ir_3Ge_5$ as the nonmagnetic counterpart to estimate the lattice contribution. We have used $La_2Ir_3Ge_5$ for the purpose since we find that in some cases the lattice contribution is overestimated if we use $Y_2Ir_3Ge_5$. For the samples with R=Er and Tm, we have used $Lu_2Ir_3Ge_5$ as the reference sample. The temperature dependence of C_p of the La, Y, Lu, and some of the magnetic samples above their magnetic transition temperatures could be fitted to the expression,

$$C_p = \gamma T + \beta T^3, \tag{6}$$

where γ is due to the electronic contribution and β is due to the lattice contribution. From the β value, we can estimate the value of the Debye temperature θ_D using the relation,

$$\theta_D = \left(\frac{12\pi^4 \ Nr \ k_B}{5\beta}\right)^{1/3}, \tag{7}$$

where N is the Avogadro's number, r is the number of atoms per formula unit, and k_B is the Boltzmann's constant. The estimated values of the Debye temperature θ_D is listed in Table IV where they are compared with the values estimated

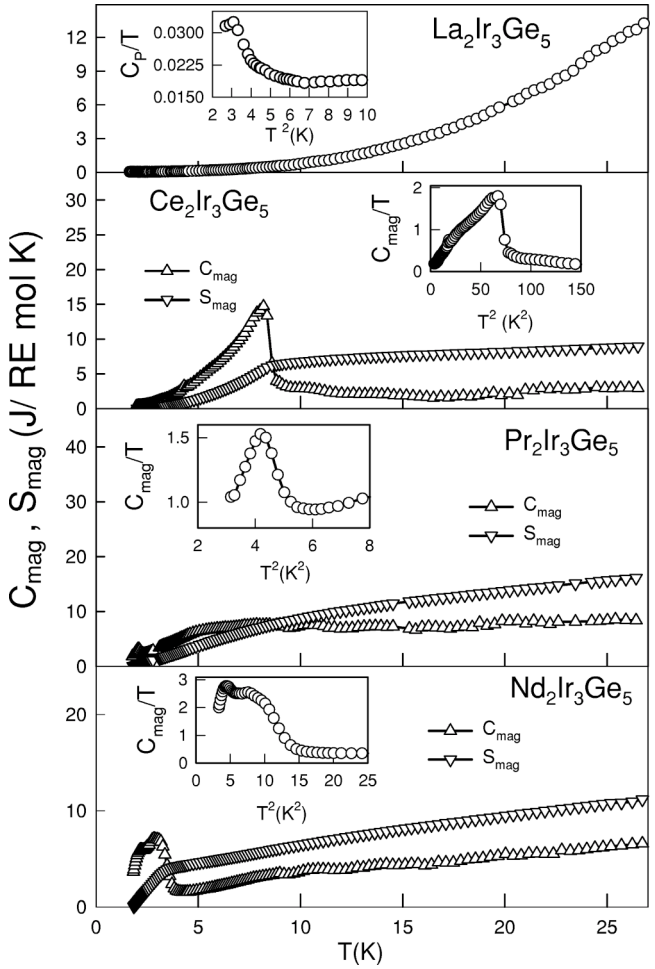

FIG. 8. Temperature dependence of the heat capacity of $R_2Ir_3Ge_5$ (R=La, Ce, Pr, and Nd) from 1.8 to 30 K. The magnetic entropy C_{mag} and the calculated values of the entropy S_{mag} (after the subtraction of the lattice contribution from C_p) are shown. The inset shows the low temperature C_p/T vs T^2 data. Large peaks observed at the respective magnetic transitions indicate bulk magnetic ordering of R^{3+} moments.

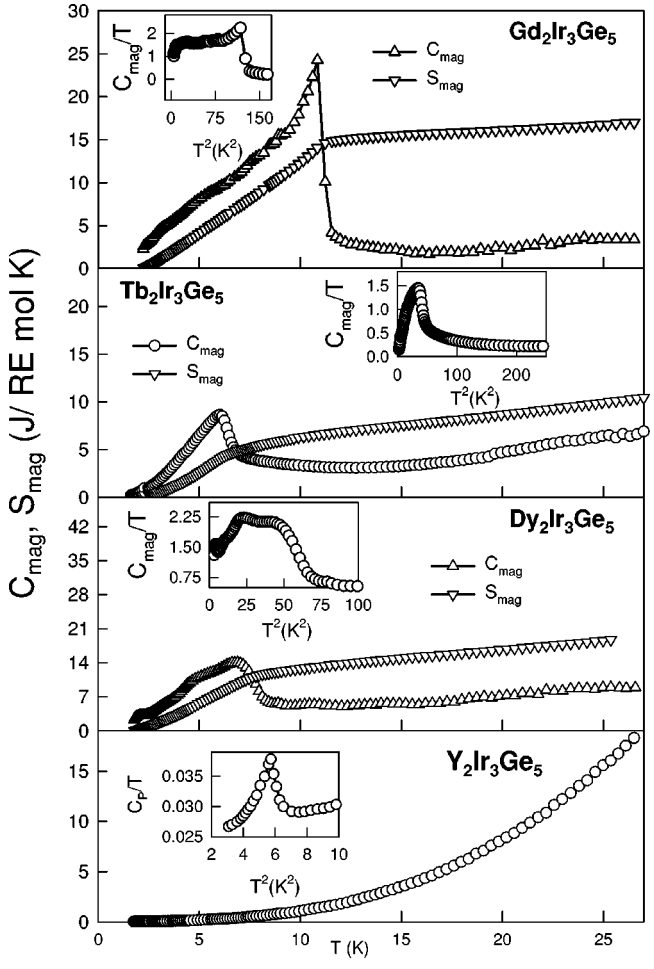

FIG. 9. Temperature dependence of the heat capacity of $R_2Ir_3Ge_5$ (R=Gd, Tb, Dy, and Y) from 1.8 to 30 K. The magnetic entropy C_{mag} and the calculated values of the entropy S_{mag} (after the subtraction of the lattice contribution from C_p) are plotted. The inset shows the low temperature C_p/T vs T^2 data. Large peaks observed at the respective magnetic transitions indicate bulk magnetic ordering of R^{3+} moments.

from the fit to the high-temperature resistivity data with the parallel resistor model. We find that for the La and Y compounds the estimated γ values are 16 mJ/R mol K^2 and 19.4 mJ/R mol K^2, respectively, which are quite high for nonmagnetic samples and could possibly indicate a large density of states at the Fermi level. The absence of superconductivity in $Lu_2Ir_3Ge_5$ above 2 K is attributed to its relatively low γ value which we found to be 9 mJ/Lu mol K^2.

The temperature dependence of C_{mag} from 1.8 to 30 K of $Ce_2Ir_3Ge_5$ is shown in Fig. 8. The inset shows the C_{mag}/T vs T^2 data at low temperatures. The large peak seen at 8.3 K in the inset confirms the bulk ordering of the Ce^{3+} moments. This temperature is comparable to the values of the transition temperature as obtained by the χ and $\rho(T)$ measurements. This transition temperature also closely resembles the previously reported values.[15] It must be noted that we observe a small shoulder at 4.3 K in the C_{mag} (see the small kink in the inset) data where we had observed a strong ferromagnetic upturn in the χ data. The extrapolated value for the Sommerfield's electronic heat-capacity coefficient γ was found to be 188 mJ/Ce mol K^2 which classifies it as a moderately heavy fermion system. However, estimation of γ from data above T_N can be easily influenced by magnetic correlations and CEF effects and may not be strictly correct. For a correct estimation of the true value of γ, data down to much lower temperatures would be required. The estimated entropy at 30 K is found to be 8.83 J/ Ce mol K which is much less than the expected value of $R\ln(2J+1)$ (with $J=5/2$ for Ce). The reduced value of the entropy implies that there are higher lying CEF levels which have not been populated at these temperatures and so the whole entropy is not released. The Kondo effect seen in the resistivity data could also be partly responsible for the reduced entropy. The experimentally obtained values of the entropy and the expected values have been compared for all compounds in Table V.

The temperature dependence of C_{mag} from 1.8 to 30 K of $Pr_2Ir_3Ge_5$ is also shown in Fig. 8. The inset clearly shows a distinct peak at a T^2 value corresponding to a temperature

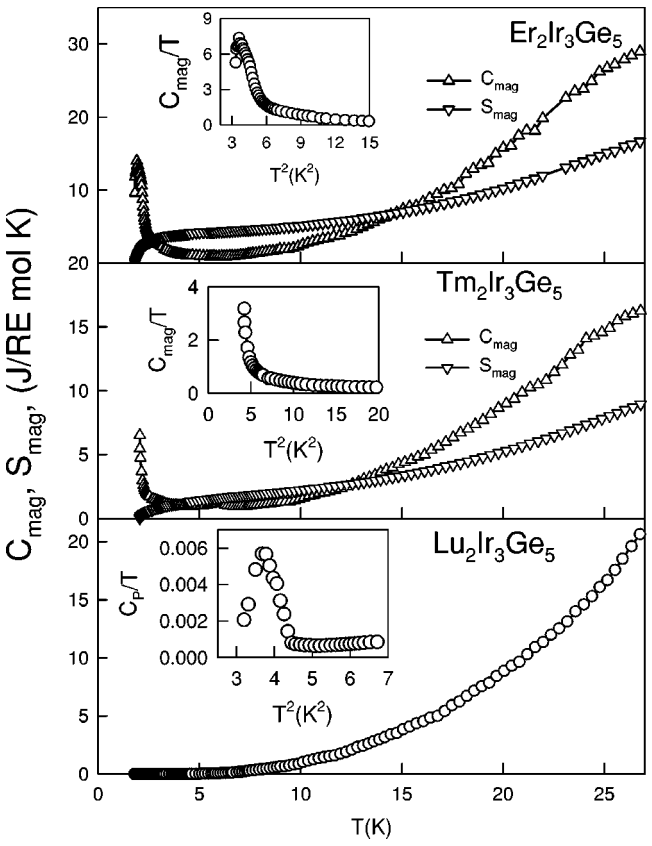

FIG. 10. Temperature dependence of the heat capacity of $R_2Ir_3Ge_5$ (R=Er, Tm, and Lu) from 1.8 to 30 K. The magnetic entropy C_{mag} and the calculated values of the entropy S_{mag} (after the subtraction of the lattice contribution from C_p) are shown. The inset shows the low temperature C_p/T vs T^2 data. The incomplete peaks in the insets for the Er and Lu samples show the magnetic and superconducting transitions, respectively. Onset of magnetic order is also seen at low temperatures for the Tm compound.

just above 2 K. This anomaly in the heat capacity, along with the peak in the susceptibility data at a similar temperature clearly establishes bulk antiferromagnetic ordering for the compound although we did not see any change in slope in the resistivity data down to 1.7 K. We observe a broad hump around 7 K in the C_{mag} data. This could be a Schottky type anomaly indicating the presence of low-lying excited CEF levels which become populated as the temperature is increased. Similar behavior has been observed in many other Pr based compounds like $Pr_2Rh_3Si_5$ (Ref. 4) and $Pr_2Rh_3Sn_5$.[18] For the former case the authors have used a singlet ground state and a doublet excited state for the CEF levels to explain the data. The estimated entropy of 15.8 J/Pr mol K at 30 K is again found to be less than the expected value of $R\ln(2J+1)$ clearly suggesting the influence of CEF levels at these temperatures.

TABLE V. Parameters obtained from the fit of the high temperature (75–300 K) $\rho(T)$ data to the parallel resistor model in $R_2Ir_2Ge_5$. θ_D(HC) is the value estimated from heat-capacity studies.

Sample	ρ_{max} $\mu\Omega$ cm	ρ_0 $\mu\Omega$ cm	C1 $\mu\Omega$ cm	θ_D(fit) (K)	θ_D(HC) (K)
$Y_2Ir_3Ge_5$	335	53	824	376	318
$La_2Ir_3Ge_5$	572	40	1337	433	319
$Pr_2Ir_3Ge_5$	744	48	781	266	289
$Nd_2Ir_3Ge_5$	749	51	865	324	287
$Gd_2Ir_3Ge_5$	258	100	394	214	232
$Tb_2Ir_3Ge_5$	548	99	532	206	247
$Dy_2Ir_3Ge_5$	487	128	1169	362	337

The temperature dependence of C_{mag} from 1.8 to 30 K of $Nd_2Ir_3Ge_5$ (Fig. 8) shows two distinct and separate anomalies (seen more clearly in the C_{mag}/T vs T^2 inset) at 2 K and 2.8 K corroborating the two anomalies seen earlier in the $d\chi/dT$ plot. The estimated entropy at 30 K in this case is again much lower than the expected value of $R\ln(2J+1)$ (see Table V).

The temperature dependence of the heat capacity for $Gd_2Ir_3Ge_5$ from 1.8 to 30 K is shown in Fig. 9. We observe a large λ type anomaly at 11.2 K which clearly indicates bulk magnetic ordering of Gd^{3+} moments. A broad shoulder is also visible at 4.2 K which corresponds with the second peak seen earlier in the χ and $d\rho/dT$ data at roughly the same temperature. This second anomaly can be associated with the way the $(2J+1)$ multiplet under consideration evolves within the ordered state. This low-temperature hump following a magnetic transition at a higher temperature has been seen in some other Gd based compounds such as GdBiPt (Ref. 21) and $GdCu_2Si_2$.[24] The inset with the low temperature C_{mag}/T vs T^2 data shows the two anomalies more clearly. The estimated entropy at 30 K is found to be 16.8 J/Gd mol K which is nearly equal to the expected value of $R\ln(2J+1)$. Note that at T_N the entropy has already reached 88% of its value at 30 K.

The data for $Tb_2Ir_3Ge_5$, also shown in Fig. 9 show a huge (10 J/Tb mol) peak at the magnetic ordering temperature of 6 K. The magnetic heat capacity shows what looks like the low-temperature tail of a Schottky like hump around 29 K. The reduced entropy value at 30 K is indicative of CEF effects being important at these temperatures.

The C_{mag} vs T data for $Dy_2Ir_3Ge_5$ shown in the same figure shows three distinct anomalies at 2.1 K, 4.8 K, and 7.4 K. We had also seen three anomalies at roughly these temperatures in the $d\chi/dT$ and $d\rho/dT$ plots for this sample. These features below the first main transition could be due to reorientation of the spins in the ordered state. Usually the change is small enough to escape a distinct detection in a magnetic measurement. However, in the reorientation of spins, some degree of freedom is involved and hence a signature in the heat capacity. Reorientation of spins is just a conjecture at the present time and it is possible that this compound actually has a complicated magnetic structure at low temperatures. This issue can be settled with neutron diffraction to probe the low-temperature magnetic structure and the changes it undergoes across the three transitions. The last panel in the same figure shows the C_P data for $Y_2Ir_3Ge_5$. The inset showing the C_P/T vs T^2 data at low temperatures shows an anomaly peaked at $T^2=6$ K^2 which corresponds to the superconducting transition seen at 2.5 K in the ρ and χ

measurements. The value of $\delta C/\gamma T_C$ is found to be 0.64 which is much reduced from the value 1.43 for a BCS type superconductor. This indicates that $Y_2Ir_3Ge_5$ may be a weakly coupled superconductor.

Figure 10 shows the heat-capacity data for the compounds $R_2Ir_3Ge_5$ (R=Er, Tm, Lu) forming in the crystal structure different from the rest of the compounds. The C_{mag} data for $Er_2Ir_3Ge_5$ show an upturn at low temperatures starting at 6 K and undergoes a maximum peak around 1.9 K. However, we could not trace the complete transition down to lower temperatures because of experimental limitations. This corresponds with the anomalies seen in the $d\chi/dT$ and ρ data discussed earlier.

The data for $Tm_2Ir_3Ge_5$ seen in the same figure also show an upturn below 3.5 K which continues down to 1.8 K. This may be the onset of the magnetic ordering of Tm^{3+} moments in this sample which we have not been able to capture because of the transition being below 2 K. The estimated entropy of only 9.2 J/Tm mol K at 30 K is much reduced from the expected value of $\ln(2J+1)$ (with $J=6$ for Tm). However, it must be noted that we see a strong indication that the compound may order below 2 K and a lot of entropy would be sitting under the peak at the transition when it occurs. The heat-capacity data for $Lu_2Ir_3Ge_5$ is also shown in Fig. 10. The C_P vs T^2 inset shows an incomplete anomaly around 2 K which corresponds with the abrupt drop in resistivity at the same temperature and could be a signature of superconductivity in this compound although we could not observe any diamagnetic signal in our magnetic measurements down to 1.8 K.

IV. DISCUSSION

In this section we will make an attempt to understand the temperature dependence of the measured physical properties and the models which we have used to understand their behavior and look for systematic trends followed across the series. We begin with the susceptibility behavior. The high-temperature data for all samples could be fitted to a modified Curie-Weiss law. The extracted effective moments for all samples are close to their theoretical values for free R^{3+} ions showing that we are dealing with trivalent moments here and that there is no contribution from the Ir. It must be recalled that the $Yb_2Ir_3Ge_5$ sample showed a much reduced moment estimated from the high-temperature data and that was attributed to the fact that the rare-earth element has two inequivalent sites in the crystal structure and so the Yb could have a different valence at the two sites.[16] We see here that both the Er and Tm samples, which form in the same crystal structure as the Yb sample show trivalent behavior with $Er_2Ir_3Ge_5$ undergoing magnetic ordering below 2 K as seen in the heat capacity and resistivity measurements while $Tm_2Ir_3Ge_5$ is also seen to be on the verge of magnetic order and we can already see the onset in the low-temperature heat-capacity inset for the sample. From Table I it can be seen that the temperature independent susceptibility χ_0 is non-negligible for some cases which possibly indicates a large density of states at the Fermi level $N(E_F)$. The values of θ_P are found to be of the order of -15 K (see Table I) for most of the compounds. These values are significantly higher than those of $R_2Rh_3Sn_5$ (Ref. 18) for example. This explains the higher values of the T_N's of the compounds of the $R_2Ir_3Ge_5$ series. The data begins to deviate from the Curie-Weiss behavior at lower temperatures because of the influence of crystalline electric fields and because of the growing of magnetic correlations. In the section where we described the results from susceptibility measurements we mentioned that we have used the $d(\chi T)/dT$ vs T plots to determine the antiferromagnetic transition temperatures. Near an antiferromagnetic transition the temperature dependence of $d(\chi T)/dT$ mimics the magnetic heat capacity curve.[25] This was demonstrated beautifully in Fig 3 where we had plotted $d(\chi T)/dT$ vs T for $Nd_2Ir_3Ge_5$ and $Dy_2Ir_3Ge_5$. Comparing this curve with the magnetic heat capacity of $Nd_2Ir_3Ge_5$ and $Dy_2Ir_3Ge_5$, one can see a clear similarity in the shape of the curves near the various transitions. The transition temperatures, however, can be deduced unambigously by this method only by taking into account data from other measurements also because taking the derivative sometimes gives some spurious peaks and in general the noise is enhanced in the derivative and so one has to be careful in determining T_N by this method. We now turn our attentions to the resistivity data. From Table III it can be seen that most of the samples have resistivity values typical of rare-earth intermetallic compounds at low-temperatures. The power-law fit to the low-temperature data for $La_2Ir_3Ge_5$ and $Y_2Ir_3Ge_5$ in their normal state as described in the Section III B shows that the data deviate from the expected T^3 dependence predicted by the Wilsons s-d scattering model. There are cases of many nonmagnetic intermetallic alloys where the low temperature resistivity data deviates from the T^3 dependence and follow a power-law behavior with $n<3$. However, it is difficult to find many compounds showing $n>3$ as we find for both $La_2Ir_3Ge_5$ and $Y_2Ir_3Ge_5$. The reasons are not well understood at present but could be due to lattice anharmonicity or phonon drag effects. Attempts to fit the resistivity data in the paramagnetic region for the compounds containing magnetic rare-earth show that only $Gd_2Ir_3Ge_5$ follows a T^2 dependence suggesting dominance of scattering by spin fluctuations at these temperatures for this compound. Both $Tb_2Ir_3Ge_5$ and $Dy_2Ir_3Ge_5$ show a power-law behavior with $n=2.1$ which is close to the T^2 dependence. However, for both $Pr_2Ir_3Ge_5$ and $Nd_2Ir_3Ge_5$ we find a marked deviation from the T^2 law with n being equal to 2.4 and 1.7, respectively. These $T^{2.4}$ and $T^{1.7}$ dependences for ρ at low temperatures is quite puzzling and not understood at present. The $Ce_2Ir_3Ge_5$ compound shows heavy fermion behavior and the expected T^2 behavior might occur at very low temperatures. We could also fit the data below T_N for many magnetic samples to a power-law dependence. The values of $n>1$ found for most of the samples except $Gd_2Ir_3Ge_5$ ($n<1$) is expected below the antiferromagnetic ordering. The fractional temperature dependence of ρ below T_N for $Gd_2Ir_3Ge_5$ can be attributed to the scattering of conduction electrons by critical spin fluctuations which begin to grow as one approaches T_N. Such a behavior has also been observed earlier in other Gd based samples such as $Gd_2Rh_3Sn_5$.[18] One clearly needs more studies on these com-

TABLE VI. Parameters obtained from the heat-capacity measurements on $R_2Ir_3Ge_5$.

Sample	T_N(K)	S_{mag} (T_N [a])/R	J	ln(2J+1)	S_{mag}(30 K)/R
$Ce_2Ir_3Ge_5$	8.7	0.678	$\frac{5}{2}$	1.79	1.08
$Pr_2Ir_3Ge_5$	2.04	0.05	4	2.19	1.94
$Nd_2Ir_3Ge_5$	2.08,2.75 [b]	.506	$\frac{9}{2}$	2.30	1.29
$Gd_2Ir_3Ge_5$	4.5,11.21 [b]	1.76	$\frac{7}{2}$	2.08	2.02
$Tb_2Ir_3Ge_5$	6.0	0.59	6	2.57	1.53
$Dy_2Ir_3Ge_5$	2.07,4.79,7.3 [b]	1.4	$\frac{15}{2}$	2.77	2.25
$Er_2Ir_3Ge_5$	1.91	0.45	$\frac{15}{2}$	2.773	1.82
$Tm_2Ir_3Ge_5$	2.3	0.144	6	2.56	1.10

[a]Multiple transitions.

[b]Transition temperatures are determined from C_p data.

pounds to try to understand their transport properties and clean single crystals would be helpful in doing so because it is well known that in ternary silicides and germanides the transport properties can be highly anisotropic and the overall behavior for a polycrystalline sample can be easily influenced by this. The semiconducting behavior in the resistivity for the samples $Er_2Ir_3Ge_5$, $Tm_2Ir_3Ge_5$, and $Lu_2Ir_3Ge_5$ is interesting. In our recent report on the sample $Yb_2Ir_3Ge_5$ we had found a metallic resistivity in the same temperature range.[16] A similar behavior in the transport properties has been observed in $R_3Ru_4Ge_{13}$ (Ref. 20) and RBiPt (Ref. 21) where the resistivity for all samples except Yb showed a semiconducting response. However, one major difference between the behavior we observe is that there is no evidence for a gap or pseudogap as seen in these compounds since our data do not follow an activated behavior for $\rho(T)$. This is shown in Fig. 5 where we have plotted $\ln\rho$ vs $1/T$ for the Er, Tm, and Lu samples in the region where we observe a semiconducting behavior. In this respect the $\rho(T)$ behavior for our samples is similar to that of URh_2Ge_2 (Ref. 26) where a negative temperature coefficient of resistivity is found up to room temperature for some samples. We believe that like in the case of URh_2Ge_2, the anomalous resistivity behavior is arising due to crystallographic disorder which occurs due to intersite exchange between Ir and Ge. Electronic localization effects induced due to this disorder could be the origin of the weak negative temperature coefficient of resistivity in these compounds. Further investigations are definitely required to understand this behavior. We could fit the high-temperature dependence of ρ for the samples which showed metallic behavior to the parallel resistor model (see Table IV) successfully and the θ_D values obtained from such fits agree roughly with those obtained from heat-capacity data for almost all compounds (magnetic or nonmagnetic). The reasons for the difference of about 10–20 % could be due to anharmonic contribution to the transport which is not considered in the parallel resistor model. The values of ρ_{max} also vary considerably across the series and are quite high in some cases. The exact origin of the ρ_{max} is still not understood properly but it is seen that saturation occurs invariably for metals and alloys which have a large resistivity. In the semiclassical theory the resistivity is given in terms of the mean-free path λ by $\rho = 3\pi h/e^2K_F^2\lambda$. The saturation resistivity in this scheme can be obtained by putting the mean free path equal to the interatomic distance since the electrons can be scattered at most at every atom. This value of ρ_{max} is called the Ioffe-Regel resistivity after the people who proposed this. The Ioffe-Regel resistivity for most compounds is about 150–200 $\mu\Omega$ cm. However, a very recent work[28] has shown that some systems with large resistivities saturate at much larger values than the Ioffe-Regel resistivity. It can be seen from Table IV that the ρ_0's for our samples are infact quite large.

Thus it is clear that both the low-temperature and the high-temperature behavior of the transport properties for these compounds require more investigations for a better understanding.

The parameters obtained from the analysis of the heat capacity measurements can be found in Table VI where we have listed the values of the ordering temperature T_N, entropy $S_{mag}(T_N)/R$, J,ln(2J+1) and S(30 K)/R. From the column giving values of $S_{mag}(T_N)/R$ one can see that for $Ce_2Ir_3Ge_5$, $Tb_2Ir_3Ge_5$, and $Er_2Ir_3Ge_5$, the entropy just above the transition reaches a value which is close to $\ln 2$ indicating that the ground state for these compounds is a doublet. The entropy for $Ce_2Ir_3Ge_5$ increases only weakly after the transition up to about 30 K indicating that the ground-state doublet is well separated from the excited crystal field levels. The entropy value for $Nd_2Ir_3Ge_5$ reaches a value of $0.506R$ ($\approx$ 75% $R\ln 2$) at T_N and then approaches $1.34R$ ($\approx R\ln 4$) at 30 K. Given that Nd is a Kramer's ion, these values indicate that a pair of doublet ground states dominate the low temperature properties of this compound. The entropy for $Dy_2Ir_3Ge_5$ reaches a value of $1.4R$ ($\approx R\ln 4$) at T_N which indicates that the ground state is a quartet for this compound. The entropy at T_N for $Gd_2Ir_3Ge_5$ is already $1.8R$ and reaches almost the full $2.08R$ at 30 K. The entropy at T_N for $Pr_2Ir_3Ge_5$ is unusually low at $0.05R$ and is quite puzzling. The entropy reaches almost $R\ln 3$ at 10 K after the Schottky anomaly which is peaked at 5 K. This would have been consistent with a nonmagnetic CEF

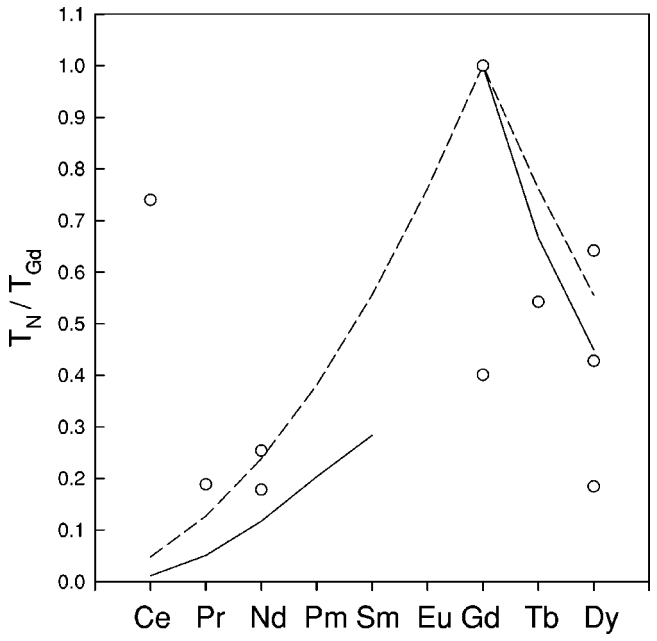

FIG. 11. Plot of the ordering temperatures of the compounds of the series $R_2Ir_3Ge_5$ (R=Ce, Pr, Nd, Tb, Gd, and Dy) normalized to the T_N value for Gd. The dashed lines represent scaling law where only spin quantum number S is used whereas the solid lines are for scaling law using total quantum number J (de Gennes scaling, see text for details).

ground state with a doublet forming the first excited state or maybe two singlets close together. However, we do see a magnetic transition in both the susceptibility and heat-capacity measurements. The reason for this unusually small entropy at the transition is not understood at present. The entropy for most of the samples continues to rise above T_N, indicating the participation of excited crystal-field levels in this temperature range, but reach values considerably reduced from the full $R\ln(2\,J+1)$.

In general, if CEF effects are not taken into account, the antiferromagnetic ordering temperature T_M for a series of isostructural and isoelectronic metals are expected to scale (de Gennes scaling[27]) as $(g_J-1)^2\,J(J+1)$ where g_J is the Lande g factor and J is the total angular momentum of the local moment. If the angular momentum is quenched then T_Ns are expected to scale as $S(S+1)$.

The solid line in Fig. 11 is the dG factor $(g_J-1)^2\,J(J+1)$ normalized to the value for Gd. The dashed line is obtained by similar normalization for the case where the orbital angular momentum L is quenched and S is the good quantum number. From Fig. 11, it is evident that the ordering temperatures (highest transition temperature for samples with multiple transitions) of the compounds roughly follow the de Gennes scaling $[(g_J-1)^2\,J(J+1)]$. The slight difference is probably due to CEF effects which are quite strong as we saw in our heat-capacity measurements. The fact that most of the compounds follow the de Gennes scaling implies that the main interaction leading to the magnetic transitions in this series may be the Ruderman-Kittel-Kasuya-Yosida (RKKY) interaction. It is worthwhile to note that the T_N for Ce (=8.5 K) is anomalously large compared to the other compounds.

V. CONCLUSION

To conclude, we have synthesized and studied compounds of the series $R_2Ir_3Ge_5$ with R=Y, La, Ce–Nd, Gd–Tm, and Lu using x-ray powder diffraction, magnetic susceptiblity, isothermal magnetization, electrical resistivity, and heat-capacity measurements. We find that the crystal structure changes from a tetragonal $U_2Co_3Si_5$ type structure for Y, La, and Ce–Dy to a different orthorhombic structure with space group *Pmmn* for Er–Lu. The nonmagnetic compounds $La_2Ir_3Ge_5$ and $Y_2Ir_3Ge_5$ show superconductivity below 1.8 K and 2.4 K, respectively, while for the compound $Lu_2Ir_3Ge_5$ indications for superconductivity could be seen in the resistivity and heat-capacity measurements only. The absence of bulk superconductivity above 2 K for this compound may be attributed to the low density of states at the fermi level for the Lu compound as indicated by the small value of the Sommerfield's coefficient for this compound compared to the Y and La compounds. All compounds containing magnetic rare-earth elements were found to give an estimated effective moment μ_{eff} close to the free ion R^{3+} values and show magnetic ordering below 12 K or onset of magnetic order as in the case of $Tm_2Ir_3Ge_5$. $Dy_2Ir_3Ge_5$, $Nd_2Ir_3Ge_5$, and $Gd_2Ir_3Ge_5$ show multiple transitions apart from the main antiferromagnetic transition. The ordering temperature of $Ce_2Ir_3Ge_5$ at 8.5 K is anomalously high compared to the other compounds considering that $Gd_2Ir_3Ge_5$ orders at 12 K. $Ce_2Ir_3Ge_5$ shows a Kondo-lattice behavior with a doublet ground state and moderate heavy electron behavior. The $T^{3.6}$ and $T^{3.3}$ power-law behavior of the normal state ρ data for $La_2Ir_3Ge_5$ and $Y_2Ir_3Ge_5$, respectively, and the $T^{2.4}$ and $T^{1.7}$ power-law dependence of the ρ data in the paramagnetic state for $Pr_2Ir_3Ge_5$ and $Nd_2Ir_3Ge_5$ is not understood at present. We find a semiconducting resistivity for the compounds $Er_2Ir_3Ge_5$, $Tm_2Ir_3Ge_5$, and $Lu_2Ir_3Ge_5$ which we believe is arising due to crystallographic disorder caused by an inter-site exchange between the Ir and Ge. The transport properties for this series of compounds clearly merits and requires further investigations on cleaner samples and preferably on single crystals to investigate the role of anisotropy on the overall behavior of ρ. From the temperature dependence of the entropy for the various compounds we have been able to establish that the ground state for the compounds $Ce_2Ir_3Ge_5$, $Nd_2Ir_3Ge_5$, $Tb_2Ir_3Ge_5$, and $Er_2Ir_3Ge_5$ is a doublet while the ground state for $Dy_2Ir_3Ge_5$ is a quartet. We could also observe the complete octuplet for $Gd_2Ir_3Ge_5$. It was difficult to establish the ground states for $Pr_2Ir_3Ge_5$ and $Tm_2Ir_3Ge_5$ compounds given that the Tm compound does not order down to the lowest temperatures of our measurements and the Pr compound shows an anomalously low entropy above the magnetic transition. Finally, the transition temperatures for most of the compounds scale with the de Genne's factor indicating that the chief mechanism through which the magnetic moments interact may actually be the RKKY type.

[1] P. Rogl, in *Handbook of Physics and Chemistry of Rare Earths*, edited by K.A. Gschneidner, Jr. and L. Eyring (Elsevier, Amsterdam, 1984), Vol. 7, pp. 1–264.
[2] J. Leciejewicz and A. Szytula, in *Handbook of Physics and Chemistry of Rare Earths*, edited by K.A. Gschneidner, Jr. and L. Eyring (Elsevier, Amsterdam, 1989), Vol. 12, p. 133.
[3] C. Mazumdar, K. Ghosh, R. Nagarajan, S. Ramakrishnan, B.D. Padalia, and L.C. Gupta, Phys. Rev. B **59**, 4215 (1999).
[4] S. Ramakrishnan, N.G. Patil, A.D. Chinchure, and V.R. Marathe, Phys. Rev. B **64**, 064514 (2001).
[5] C.B. Vining and R.N. Shelton, Phys. Rev. B **28**, 2732 (1983).
[6] H.F. Braun, Phys. Lett. **75A**, 386 (1980).
[7] H.F. Braun, C.U. Segre, F. Acker, M. Rosenberg, S. Dey, and U. Deppe, J. Magn. Magn. Mater. **25**, 117 (1981).
[8] A.R. Moodenbaugh, D.E. Cox, and H.F. Braun, Phys. Rev. B **25**, 4702 (1981).
[9] J.A. Gotaas, J.W. Lynn, R.N. Shelton, P. Klavins, and H.F. Braun, Phys. Rev. B **36**, 7277 (1987).
[10] C.B. Vining, R.N. Shelton, H.F. Braun, and M. Pelizzone, Phys. Rev. B **27**, 2800 (1983).
[11] S. Noguchi and K. Okuda, Physica B **194-196**, 1975 (1994).
[12] Y. Singh, S. Ramakrishnan, Z. Hossain, and C. Geibel, Phys. Rev. B **66**, 014415 (2002).
[13] G. Venturini, M. Meot-Meyer, J.F. Marcche, B. Malaman, and B. Roques, Mater. Res. Bull. **21**, 33 (1986).
[14] C. Godart, C.V. Tomy, L.C. Gupta, and R. Vijayaraghavan, Solid State Commun. **67**, 677 (1988).
[15] Z. Hossain, H. Ohmoto, K. Umeo, F. Iga, T. Suzuki, T. Takabatake, N. Takamoto, and K. Kindo, Phys. Rev. B **60**, 10 383 (1999).
[16] Yogesh Singh and S. Ramakrishnan, Phys. Rev. B **68**, 054419 (2003).
[17] S. Ramakrishnan, S. Sundaram, R.S. Pandit, and Girish Chandra, J. Phys. E **18**, 650 (1985).
[18] N.G. Patil and S. Ramakrishnan, Phys. Rev. B **59**, 12 054 (1999).
[19] Bernd Becker, Ph.D thesis, University of Netherlands, 1996.
[20] K. Ghosh, S. Ramakrishnan, and Girish Chandra, Phys. Rev. B **48**, 10 435 (1993).
[21] P.C. Canfield, J.D. Thompson, W.P. Beyermann, A. Lacerda, M.F. Hundley, E. Peterson, Z. Fisk, and H.R. Ott, J. Appl. Phys. **70**, 5800 (1991).
[22] J. M. Ziman, *Electrons and Phonons: The Theory of Transport Phenomena in Solids* (Clarendon Press, Oxford, 1960).
[23] H. Wiesmann, M. Gurvitch, H. Lutz, A. Ghosh, B. Schwarz, M. Strongin, P.B. Allen, and J.W. Halley, Phys. Rev. Lett. **38**, 782 (1977).
[24] M. Bouvier, P. Lethuillier, and D. Schmitt, Phys. Rev. B **43**, 13 137 (1991).
[25] M.E. Fisher, Philos. Mag. **7**, 1731 (1962).
[26] S. Sullow, S.A.M. Mentink, T.E. Mason, R. Feyerherm, G.J. Nieuwenhuys, A.A. Menovsky, and J.A. Mydosh, Phys. Rev. B **61**, 8878 (2000).
[27] D.R. Noakes and G.K. Shenoy, Phys. Lett. A **91**, 35 (1982).
[28] O. Gunnarson, M. Calandra, and J.E. Han, Rev. Mod. Phys. **75**, 1085 (2003).